ACS OMEGA

http://pubs.acs.org/journal/acsodf

Article

Ultrasimple and Ultrafast Method of Optical Modulation by Perovskite Quantum Dot Attachment to a Graphene Surface

Xueqiong Su,* Yong Pan, Dongwen Gao, Jin Wang, Ruixiang Chen, Yimeng Wang, Xin-yu Yang, and Li Wang*

Cite This: *ACS Omega* 2022, 7, 19606−19613

Read Online

ACCESS | Metrics & More | Article Recommendations

ABSTRACT: Optical modulation is the process of modifying the structure and elemental composition of materials so that the main optical parameters, including amplitude, frequency, and phase, are changed. Currently, much research attention has been directed toward ultrafast dynamics, but the process of modulation is often complex. To simplify the optical modulation process and improve the optical properties of perovskites for semiconductor quantum dot (QD) lasers, the process and physical mechanism underlying graphene QD ultrafast modulation of the optical properties of perovskite $CsPbBr_3$ QDs were investigated. The typical cubic structure and square shape of $CsPbBr_3$ QDs were characterized by transmission electron microscopy and X-ray diffraction, respectively. A luminescent peak centered near 540 nm and Stokes shift of 21.34 nm of $CsPbBr_3$ QDs without graphene QDs were measured by absorption and photoluminescence spectroscopy. A maximum modulation shift of 133 nm and a modulation depth of 900% were achieved in $CsPbBr_3$ with graphene. The results indicated that graphene QDs had the best modulation effect on perovskites when the drop volume was 0.05 mL. The process of ultrafast optical modulation via graphene QDs occurring within 1 ps was confirmed by the transient absorption spectrum. The modulation mechanism of graphene to perovskites is presented for guidance. This paper can be used as a reference for the optical modulation of perovskite materials.

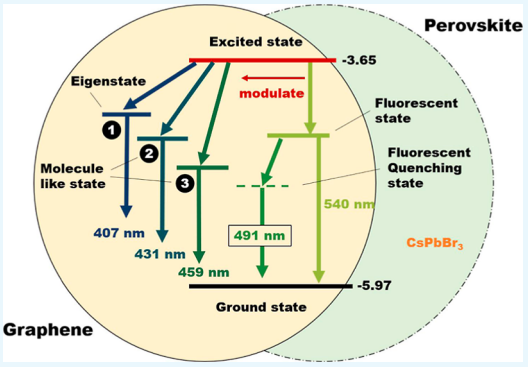

1. INTRODUCTION

Perovskite materials such as $CsPbBr_3$ have great application prospects in the active medium of lasers due to their low density of band-to-band defects, long carrier diffusion distance, high light absorption efficiency, and high luminous efficiency.[1−4] The inorganic perovskite quantum dots (QDs) have attracted attention because of their high quantum yield, large photon absorption cross section, and regulable fluorescence wavelength and have great potential as laser gain media.[5−7] Thus, many research studies have been performed in this field. A very low threshold and stable spontaneous emission amplification optical gain characteristics of perovskites were confirmed,[8] which exhibited a tunable laser wavelength with changes to the halogen component. Additionally, high *Q*-value laser emission was realized using hybrid triangular and hexagonal perovskite materials.[9] As reported in ref 10, high-intensity laser emission was obtained using a metal mirror resonator structure, and the pump light in the visible region was converted into a near-infrared laser with a conversion efficiency of up to 70%. Although the existing research has made many breakthroughs, the luminescent properties of many perovskite QDs are still not satisfactory for application. The narrow luminescence spectrum and low intensity can be considered as the obstacles to use in QD lasers. Modulation of optical properties for perovskites is the effective way to solve the problem.

At present, there are three methods used for the optical modulation of QDs, including the microstructure alterations, concentration changes, and doping modifications.[11−14] Specifically, the modification of the material microstructure to obtain different optical properties is called microstructural modification. However, this method is difficult to execute, expensive, and unstable with respect to the optical properties achieved. The method involving changes in concentration is a common way to modulate the optical properties of materials, but this method can only translate the spectrum (blue shift or red shift) and not change the intensity. Doping modification is the method of mixing particles or QD solutions with original materials to obtain optically modulated properties. As reported in ref 15, a bilateral interface modification to perovskites by doping room-temperature-synthesized $CsPbBr_3$ nanocrystals

Received: March 4, 2022
Accepted: May 26, 2022
Published: June 3, 2022

occurs, which effectively suppresses the defect at the SnO_2/perovskite interface and boosts the interfacial electron transport. In fact, the change in surface structure will eventually affect the change in microproperties of materials, such as Auger recombination. As reported in ref 16, an adjustment of the Auger recombination rate of materials through 2D iodide-perovskite nanoplatelets is seen. These studies suggest that the method of doping modification is simple, efficient, inexpensive, and flexible. In addition, different material solutions can be prepared according to different requirements and expectations. As such, we sought to employ this method to modulate the optical properties of perovskite QDs.

Graphene has been widely studied in academia and industry due to its excellent mechanical properties, ultrahigh thermal conductivity, carrier mobility, ultra-wideband optical response spectrum, and strong nonlinear optical properties.[17−19] At present, the interaction between light and graphene is a prominent research field due to the unique optical properties. Recent studies showed that the interaction between graphene and light was enhanced by surface plasmon resonance,[20−22] illustrating that the influence of graphene on light is complex and that there are many areas for further research on this topic.

In this work, an ultrasimple method for optical modulation is presented. We used graphene QDs to modulate the optical properties of perovskite QDs by attachment and achieving improved luminescence. The optical modulation ability of graphene is subsequently evaluated. In addition, the microstructure, absorption and fluorescence spectra, transient absorption (TA) behavior, and morphological characteristics are investigated. The results obtained can provide a reference for the optical properties of graphene and the modulation of optical properties.

2. EXPERIMENTAL SECTION

The $CsPbBr_3$ QD material synthesis adopted the method of hot injection, which can be seen in our previous work.[4] The concentrations of $CsPbBr_3$ and graphene were 3 and 1 mg/mL, respectively. The preparation of graphene-modulated perovskite-mixed QDs is divided into five steps. SiO_2 was selected as the substrate (Figure 1a). The dispersion with 0.05−0.15 mL of graphene QDs was dropped onto the substrate (Figure 1b). The sample was dried in air for 2−3 h until the deionized water in the graphene solution was completely evaporated (Figure 1c). The 1 mL $CsPbBr_3$ QD dispersion was then dropped on top of the layer of dried graphene QDs (Figure 1d). It is important to note that the samples had to be tested immediately after drop-coating; otherwise, the material failed.

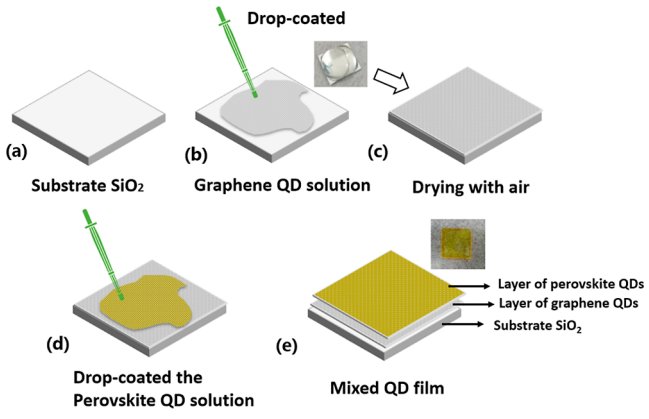

Figure 1. Preparation process for $CsPbBr_3$ and graphene-mixed QDs. (a) Substrate; (b) drop-coated graphene QD solution; (c) drying with air; (d) drop-coated perovskite QD solution; and (e) final mixed QD film.

The microstructure of the mixed QDs in the graphene-modulated perovskite was analyzed by X-ray diffraction (XRD, Bruker D8 Advance). The morphology of the QDs was visualized by transmission electron microscopy (JEM 2100). The absorption spectra were measured using a spectrometer (HITACHI U-4100). Photoluminescence (PL) was obtained by fluorescence spectroscopy (NIR512). The 355 nm pulsed laser was selected as excitation light for the PL test, which came from the NdYAG laser (spectral physics, 10 ns pulse width, and 30 Hz repetition frequency). The laser was focused on the sample, and the fluorescence was measured by the optical fiber probe of the spectrometer. TA was determined by a femtosecond laser (spectral physics, 800 nm excitation, and 150 fs pulse width). The measurement method of TA was reflective type. After the laser comes out, it passed through the broadband mirror and laser beam splitter in the reflective optical path and finally reached the sample pool. An aperture behind the sample pool was placed, and finally, a spectrometer for measurement was set.

3. RESULTS AND DISCUSSION

The TEM image of the $CsPbBr_3$ NPs is shown in Figure 2a. As seen in the image, the QDs form clusters in different areas. To observe the morphology and structure of these clusters more clearly, some of them were imaged at a higher magnification, as shown in Figure 2b. The perovskite QDs exhibit regular and uniform square shapes. The structure of the QDs can be clearly seen in Figure 2d. The ordered crystal structure was confirmed by TEM. The interatomic spacing was determined to be 5.68 Å using the calibration tool of the test equipment. However, the crystalline peaks were very weak in the XRD measurement. The samples were measured many times by XRD. The Br content was both increased and decreased, but the results were consistent.

This result can be explained by the concentration of the dispersion and the lifetime of QDs. The concentration of QD solutions is usually relatively low, which is a challenge for some QD tests. Thus, to make an accurate and reproducible measurement, it is necessary to control the instrument operation and cooperation with related instruments accurately. Although we do not have this measurement condition or feasibility to perform this operation in terms of XRD at present and the XRD signal is weak, the results show that the QDs are cubic. The typical cubic structure of the perovskite is confirmed based on both TEM and XRD observations. The structure is shown in Figure 2f. The Cs atoms occupy the four corners of the cube, the Br atoms occupy the face centers of the cube, and the Pb atom is located at the center of the unit cell. The relationship between the thickness of the graphene QD layer and their concentration is displayed in the Figure 2g. During preparation, 0.10 mL of graphene was dripped after 0.05 mL of graphene dried. Thus, the thickness of 0.10 mL is equivalent to the thickness of two layers of 0.05 mL. The size distribution of perovskite QDs is displayed in Figure 2h. The size of perovskite QDs is mainly in the range of 8−10 nm (59.2%), which represents the average size of $CsPbBr_3$ QDs prepared in this experiment.

The PL spectrum of $CsPbBr_3$ QDs without graphene is shown in Figure 3a. The results of 500−580 nm with the

https://doi.org/10.1021/acsomega.2c01310
ACS Omega 2022, 7, 19606−19613

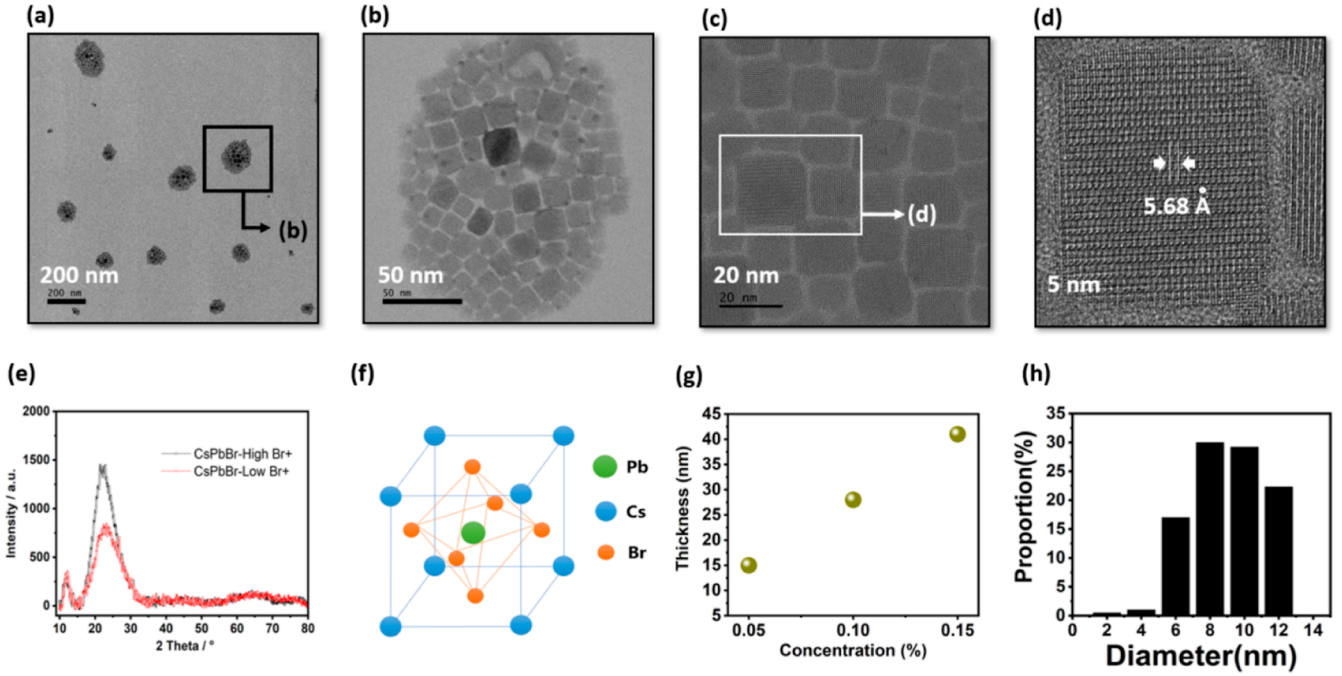

Figure 2. Morphology and structure of $CsPbBr_3$ QDs. (a–d) TEM images of $CsPbBr_3$ NPs; (e) XRD patterns for $CsPbBr_3$ QDs; (f) schematic of the cubic perovskite unit cell; (g) relationship between thickness of the graphene QD layer with their concentration; (h) size distribution of perovskite QDs.

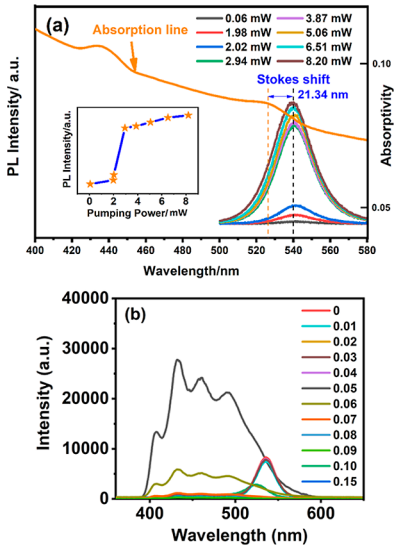

Figure 3. PL and absorption spectrum of $CsPbBr_3$ QDs with and without graphene. (a) PL (multicolor) and absorption (orange) spectra of $CsPbBr_3$ QDs without graphene. Inset plot: the relationship between PL intensity and pumping power; (b) PL spectrum with different graphene concentrations.

central peak near 540 nm luminescence are observed. The inset plot illustrates that the intensity of the PL peak increases with increasing pump power. However, the PL peak intensity changes dramatically as the pump power increases from 2.02 to 2.94 mW. This phenomenon can be explained by the unique energy level structure of perovskite QDs. There is a quasi-continuous discrete quantum energy level structure due to the quantum confinement effect, and carriers can be excited from the ground state to the excited state. In other words, fluorescence is produced through three processes. These processes include the carrier being excited from the ground state to different higher energy levels, the carrier relaxing to the lower surface defect energy level, and the carrier transitioning from the defect energy level to the ground state. When the excitation power is small, only a few carriers can absorb the energy needed for the transition. Most carriers in the quasi-transition state after absorbing energy are found. As the excitation power increases to the critical value, most of the carriers in the quasi-transition state absorb additional energy. This leads to a large-scale transition and sudden increase in the fluorescence peak intensity. The absorption spectrum of the material is also shown in Figure 3 by an orange line. The Stokes shift was determined to be 21.34 nm by calculating the difference between the absorption peak and the fluorescence peak, which is close to the value reported previously.[4,23] When the dose of graphene QDs is small (<0.04 mL), it has no effect on perovskites because too little QD dose makes the amount of photon transfer very small, based on past experience and this result. Meanwhile, when the dose of graphene QDs is relevant large (>0.06 mL), the fluorescence quenching will occur, which is the result of a large number of graphene electron collisions, see Figure 3b. In short, a specific dose of graphene will produce optical modulation.

The absorption spectrum of $CsPbBr_3$ QDs with graphene modulation is shown in Figure 4a. After graphene QD doping, a blue shift occurred in the absorption spectrum comparing $CsPbBr_3$. The reason for this change can be explained by the quantum size effect caused by the QD surface effect.[24−26] After being added, the graphene adheres to the surface of the perovskite because of the QD cluster effect, which leads to an increase in the specific surface area of QDs. Furthermore, the change in particle size of QDs with graphene is generated due to the increasing specific surface area. According to the quantum threshold limiting effect, the absorption spectrum of QDs will shift with changing QD size.

https://doi.org/10.1021/acsomega.2c01310
ACS Omega 2022, 7, 19606−19613

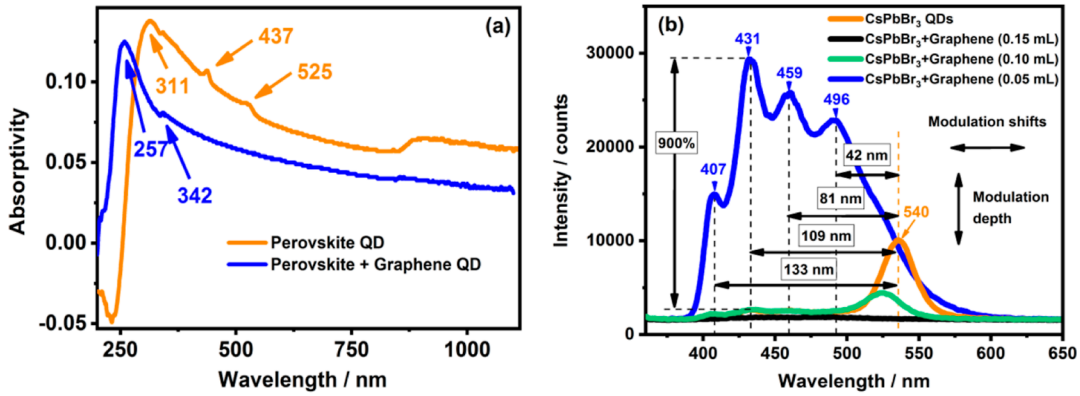

Figure 4. Absorption and PL spectra of $CsPbBr_3$ QDs with graphene. (a) Absorption spectrum of $CsPbBr_3$ QDs with and without graphene; (b) PL spectra of $CsPbBr_3$ QDs with graphene in the range of 350−650 nm.

The PL spectra of $CsPbBr_3$ with different volume additions of graphene QDs are presented in Figure 4b. The PL peak position at 540 nm for the perovskite $CsPbBr_3$ QDs without graphene is represented by an orange line. In this experiment, different concentrations (0.05, 0.10, and 0.15 mL) of graphene QDs were mixed into perovskite QDs. When the graphene volume is 0.15 mL, graphene QDs do not show optical modulation and instead exhibit a matting effect characterized by greatly decreased fluorescence intensity. When the volume of graphene QDs is reduced to 0.10 mL, the result shows a reverse modulation effect on the perovskite QDs. The fluorescence intensity of the material is reduced to half. Under these two conditions, the light modulation of graphene is not confirmed. Thus, the concentration of graphene was further reduced. Graphene shows a complete optical modulation effect on perovskite QDs when the volume of graphene QDs introduced is adjusted to 0.05 mL. The fluorescence is expanded from one peak to four, with peaks present at 407, 431, 459, and 496 nm. To explain the effect of optical modulation more clearly, the differences in peak positions (wavelengths) before and after modulation are defined as modulation shifts. Additionally, the modulation depth that expresses the intensity difference before and after modulation was determined. The largest transverse modulation shift is 133 nm, and the smallest is 42 nm. The intensity of the fluorescence peak increases by 900% for the maximum longitudinal modulation amplitude. In summary, the results of the PL spectra demonstrate that perovskite $CsPbBr_3$ QDs are best modulated when the volume of introduced graphene is 0.05 mL.

To confirm the accuracy of the results demonstrated above and the energy level structure model, TA spectra were recorded. The TA spectra of the perovskite $CsPbBr_3$ without graphene are presented in Figure 5a. The spectra show that ground-state bleaching and stimulated emission are seen in the same range due to the small Stokes shifts (20−40 nm), which is consistent with the result (21.34 nm) obtained from the absorption and PL spectra of $CsPbBr_3$. The TA and fluorescence processes in the perovskite are observed during 4000 ps in a wavelength of 535 nm, which shows good absorption and fluorescence properties. Importantly, a signal with $\Delta A > 0$, namely, the excited-state absorption (ESA) signal, is found at 500 nm, which illustrates that the excited particles at 500 nm can absorb some light that the particles in the ground state cannot, leading to their excitation to a higher energy level.[27,28] Meanwhile, the TA spectra in Figure 5b also show the corresponding stimulated emission (SE) at 500 nm after graphene modulation. However, it is detected that the SE process lasts only for 100 ps, which is similar to that observed for ESA. Thus, this process can be described as the up/down conversion of perovskite excitons. TA spectra confirmed the ESA signal of the perovskite exciton at 500 nm. However, the ESA signal is converted into an SE signal after graphene modulation. This indicates that the exciton that was originally attributed to the perovskite continues to absorb energy and is converted to release energy under the influence of the graphene energy level. The converted exciton produces 496 nm SE radiation. This is consistent with the steady-state fluorescence spectrum of the material. It also proves that the modulated energy level structure model for perovskites with graphene QDs is reasonable and accurate. Excitonic bleaching dynamics (monitored at 540 nm) with and without graphene are shown in Figure 5c. The bleach recovery dynamics of $CsPbBr_3$ QDs with and without graphene at shorter time scales (1 ps in the complex and 2 ps in $CsPbBr_3$) along with the absolute bleach amplitude are shown. This process confirms the ultrafast optical modulation (1 ps) of perovskites by graphene. The response to longer delay times is displayed in Figure 5d. Figure 5c,d shows that the optical response speed of the material increases after graphene modulation. Figure 5e indicates that the material can obtain maximum absorption when the amount of graphene present is low, which is consistent with the results of the steady-state fluorescence spectrum.

The process of modulation is depicted in Figure 6a. Modulation characteristics are not produced as perovskites and graphene are separated. Then, the graphene QDs are adsorbed to perovskite QDs after the two QD solutions mixed. Thus, the energy level interaction will be generated. The reason for stokes shift modulation is as follows: the energy levels of graphene QDs and perovskite QDs cross, and a new energy level transition is generated, so a new wavelength radiation appears. In other words, the reason of Stokes modulation is the interactive transition of energy levels. The reason for depth modulation is as follows: some electrons in graphene will transition to the original radiation level of perovskites, which enhances the original radiation and modulates the depth. To illustrate the mechanism by which graphene optically modulates perovskites, the energy levels of mixed perovskites and graphene QDs are established, as shown in Figure 6b. The reason for the disappearance of the perovskite PL peak at 540 nm after modulation can be

https://doi.org/10.1021/acsomega.2c01310
ACS Omega 2022, 7, 19606−19613

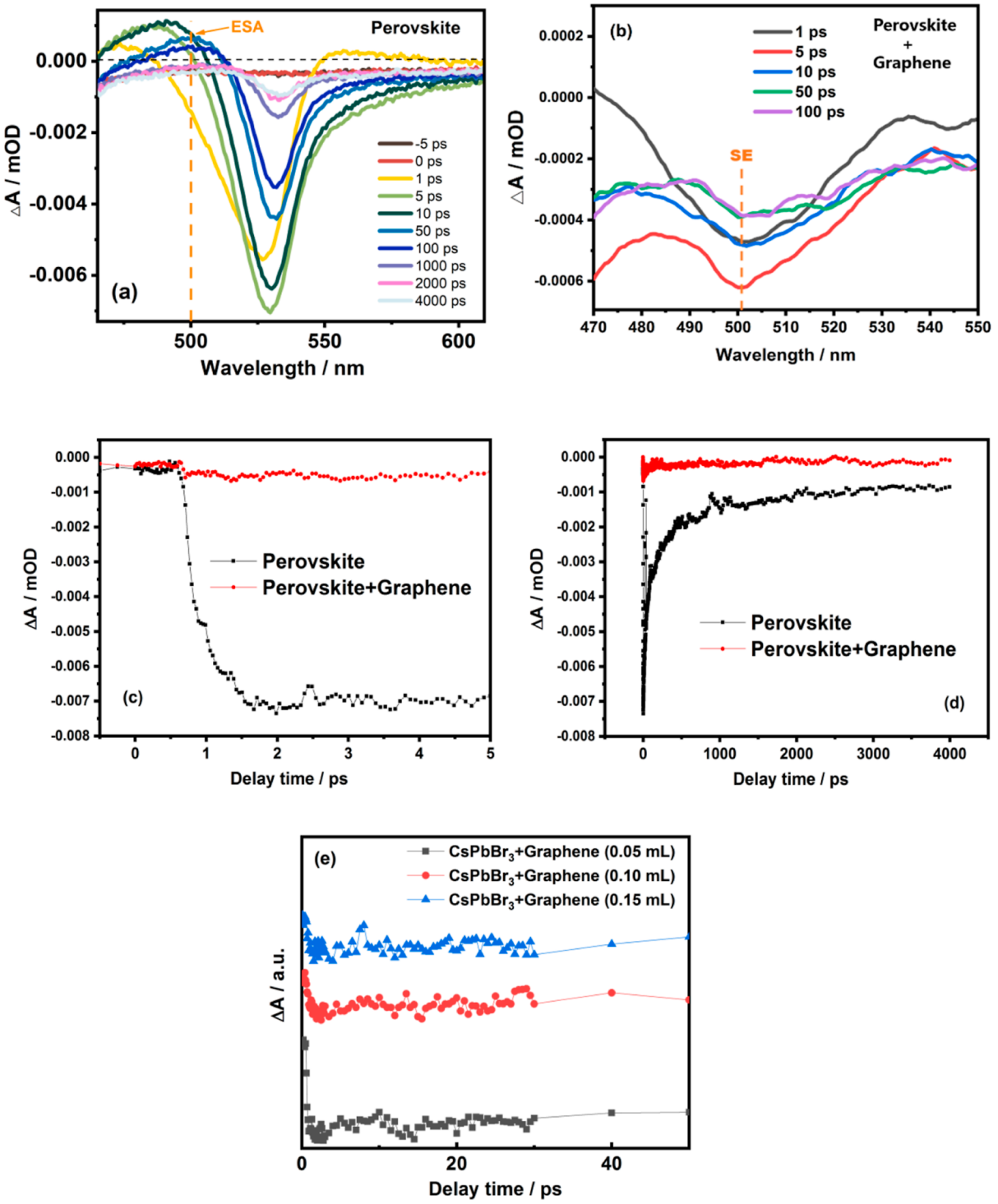

Figure 5. TA spectra at the indicated delay times following 365 nm excitation of the perovskite with and without graphene. (a) $CsPbBr_3$; (b) $CsPbBr_3$+Graphene; (c) delay time with ΔA in the range of 0−5 ps; (d) delay time with ΔA in the range of 0−4000 ps; (e) delay time with ΔA in the range of 0−200 ps for different volumes of introduced graphene.

explained by fluorescence quenching.[29,30] Fluorescence quenching is a process in which molecules with fluorescent characteristics interact with other molecules, resulting in fluorescence being suppressed. Under normal conditions, the electrons in the fluorescent molecules interacting with light in the ground state are excited to a higher energy level. At the same time, the electrons in the excited state are unstable, and they relax to the fluorescence emission level, which generates radiation. When the quenching agent interacts with the fluorescent molecule, a new quenching energy level is formed. The energy of this level is lower than that of the fluorescence energy level of the fluorescent molecule. In this case, the electrons in the excited state will not relax to the original fluorescence energy level but are captured by the quenching energy level before relaxing to the ground state in a nonradiative transition. Here, we believe that there is a

https://doi.org/10.1021/acsomega.2c01310
ACS Omega 2022, 7, 19606−19613

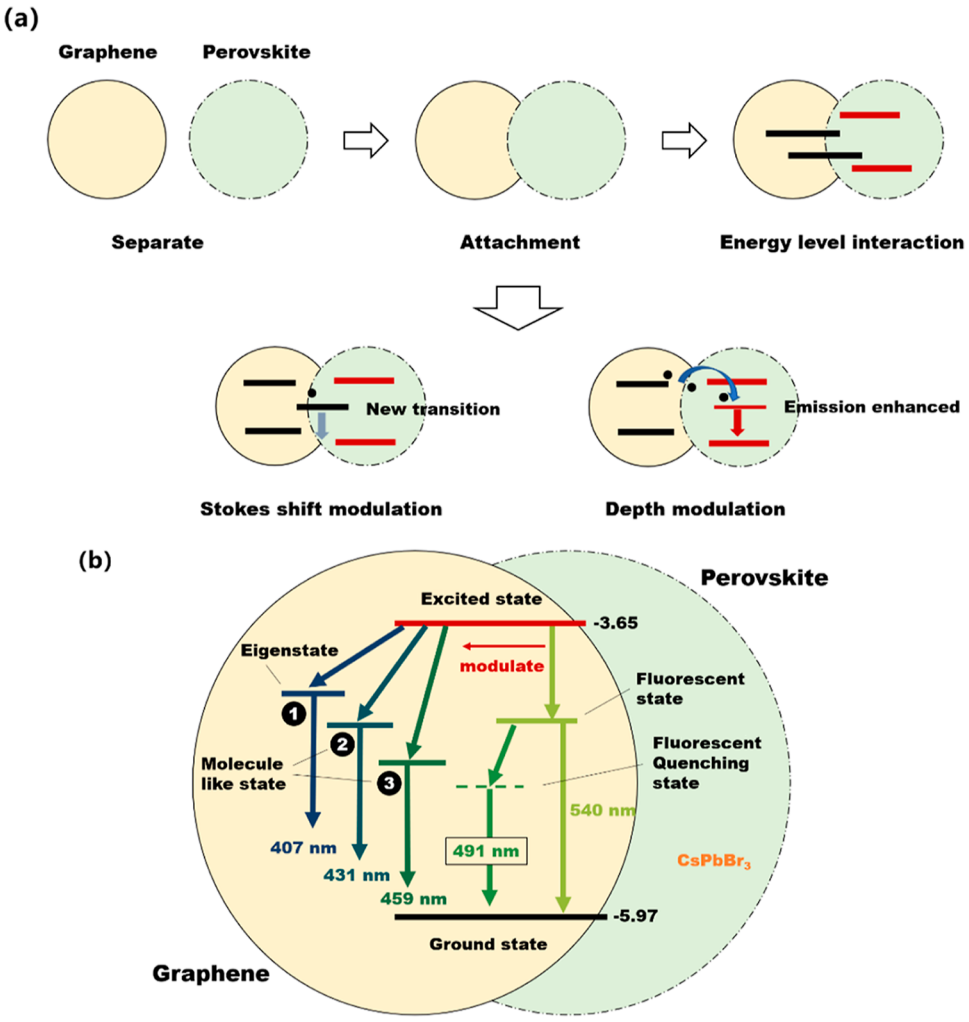

Figure 6. Modulation mechanism of graphene to perovskites. (a) Process of Stokes shift and depth modulation. (b) Energy-level structure of perovskites modulated by graphene. (SE: stimulated emission and ESA: excited-state absorption).

reabsorption-amplified spontaneous emission (ASE) conversion process occurring in samples. After absorbing the pump light, the sample transitions to the excited state, and the particles in the excited state absorb some light that cannot be absorbed by particles in the ground state. Thus, the particles in the excited state are further excited to a higher energy level.[31] Therefore, the 540 nm fluorescence peak disappears, and the 496 nm fluorescence peak is generated. In addition, the modulation must result from the interaction between the energy levels of graphene and perovskites. Through analysis of the TA and fluorescence spectra, three characteristic fluorescence states in the graphene QD system are observed. The first state is an eigenstate emitting at 407 nm that is excited by a 257 nm wavelength. The second state is a green fluorescent state emitted at 431 nm which is excited by a 257 nm wavelength. The third state is a blue fluorescent state emitted at 459 nm that is excited by a 342 nm wavelength.[32−35] The life and characteristics of the second and third fluorescent states are similar to those of molecular-like states. Therefore, graphene QDs contribute to the optical modulation of perovskite QDs.

4. CONCLUSIONS

In this paper, an ultrasimple method of perovskite QDs attached to graphene for optical modulation is presented. The process and physical mechanism by which graphene QDs modulate the optical properties of perovskite $CsPbBr_3$ QDs were investigated. The square shape and ordered crystal structure of $CsPbBr_3$ QDs were confirmed by TEM, and the cubic structure of $CsPbBr_3$ QDs was determined by XRD. Thus, based on the results of TEM and XRD, the typical cubic structure of perovskites was observed. A luminescent peak centered near 540 nm and Stokes shift of 21.34 nm for $CsPbBr_3$ QDs were measured by absorption and PL spectroscopy. Furthermore, a blue shift occurred in the absorption spectrum of $CsPbBr_3$ with graphene QDs when compared to the absorption spectrum of $CsPbBr_3$ without graphene QDs. A maximum modulation shift of 133 nm and a modulation depth of 900% were achieved by the PL spectrum. The concentration of 0.05 mL of graphene QDs showed a better modulation effect than others. Importantly, the energy level transition model of graphene-modulated perovskite QDs was established, which can be used as an explanation of the cause of modulation. Finally, the accuracy of the results and the energy level model was proven by TA measurements. The process of ultrafast optical modulation by graphene QDs required only 1

https://doi.org/10.1021/acsomega.2c01310
ACS Omega 2022, 7, 19606−19613

ps. Finally, the modulation mechanism of graphene to perovskites is presented for guidance. In conclusion, an ultrasimple and ultrafast modulation method is proven in this work. Certain concentrations of graphene QDs have an effective modulation effect on the optical properties of perovskite $CsPbBr_3$ QDs, which is beneficial for the development of perovskite QD lasers.

AUTHOR INFORMATION

Corresponding Authors

Xueqiong Su − *The School of Physics and Optoelectronics, Faculty of Science, Beijing University of Technology, Beijing 100124, China;* orcid.org/0000-0002-9763-1727; Email: nysxq@bjut.edu.cn

Li Wang − *The School of Physics and Optoelectronics, Faculty of Science, Beijing University of Technology, Beijing 100124, China*; Email: Lwang.1@bjut.edu.cn

Authors

Yong Pan − *College of Science, Xi'an University of Architecture and Technology, Xi'an 710055, China;* orcid.org/0000-0002-9647-8919

Dongwen Gao − *The School of Physics and Optoelectronics, Faculty of Science, Beijing University of Technology, Beijing 100124, China*

Jin Wang − *The School of Physics and Optoelectronics, Faculty of Science, Beijing University of Technology, Beijing 100124, China*

Ruixiang Chen − *The School of Physics and Optoelectronics, Faculty of Science, Beijing University of Technology, Beijing 100124, China*

Yimeng Wang − *The School of Optical-Electrical and Computer Engineering, The University of Shanghai for Science and Technology, Shanghai 200093, China*

Xin-yu Yang − *The College of Chemistry and Materials Engineering, Wenzhou University, Wenzhou, Zhejiang 325035, China*

Complete contact information is available at: https://pubs.acs.org/10.1021/acsomega.2c01310

Notes

The authors declare no competing financial interest.

ACKNOWLEDGMENTS

This research was supported by the National Natural Science Foundation of China under the Youth Science Foundation Project (NSFC-61805005), the Beijing University of Technology Basic Research Fund project (PXM2017-014204-500087), and the International Research Cooperation Seed Fund of Beijing University of Technology (Project no. 2021B34).

REFERENCES

(1) Zhu, H.; Yang, Y.; Lian, T. Multiexciton Annihilation and Dissociation in Quantum Confined Semiconductor Nanocrystals. *Acc. Chem. Res.* **2013**, *46*, 1270−1279.

(2) Klimov, V. I.; Mikhailovsky, A. A.; McBranch, D. W.; Leatherdale, C. A.; Bawendi, M. G. Share on Quantization of Multiparticle Auger Rates in Semiconductor Quantum Dots. *Science* **2000**, *287*, 1011−1013.

(3) Pan, Y.; Wang, L.; Su, X.; Gao, D.; Cheng, P. Nanolasers Incorporating $Co_xGa_{0.6-x}ZnSe_{0.4}$ Nanoparticle Arrays with Wavelength Tunability at Room Temperature. *ACS Appl. Mater. Interfaces* **2021**, *13*, 6975−6986.

(4) Protesescu, L.; Yakunin, S.; Bodnarchuk, M. I.; Krieg, F.; Caputo, R.; Hendon, C. H.; Yang, R. X.; Walsh, A.; Kovalenko, M. V. Nanocrystals of Cesium Lead Halide Perovskites ($CsPbX_3$, X = Cl, Br, and I): Novel Optoelectronic Materials Showing Bright Emission with Wide Color Gamut. *Nano Lett.* **2015**, *15*, 3692−3696.

(5) Yakunin, S.; Protesescu, L.; Krieg, F.; Bodnarchuk, M. I.; Nedelcu, G.; Humer, M.; De Luca, G.; Fiebig, M.; Heiss, W.; Kovalenko, M. V. Low-threshold amplified spontaneous emission and lasing from colloidal nanocrystals of caesium lead halide perovskites. *Nat. Commun.* **2015**, *6*, 8056.

(6) Tan, Z.-K.; Moghaddam, R. S.; Lai, M. L.; Docampo, P.; Higler, R.; Deschler, F.; Price, M.; Sadhanala, A.; Pazos, L. M.; Credgington, D.; Hanusch, F.; Bein, T.; Snaith, H. J.; Friend, R. H. Bright light-emitting diodes based on organometal halide perovskite. *Nat. Nanotechnol.* **2014**, *9*, 687−692.

(7) Pan, Y.; Huang, L.; Sun, W.; Gao, D.; Li, L. Invisibility Cloak Technology of Anti-Infrared Detection Materials Prepared Using CoGaZnSe Multilayer Nanofilms. *ACS Appl. Mater. Interfaces* **2021**, *13*, 40145−40154.

(8) Xing, G.; Mathews, N.; Lim, S. S.; Yantara, N.; Liu, X.; Sabba, D.; Grätzel, M.; Mhaisalkar, S.; Sum, T. C. Low-temperature solution-processed wavelength-tunable perovskites for lasing. *Nat. Mater.* **2014**, *13*, 476−480.

(9) Zhang, Q.; Ha, S. T.; Liu, X.; Sum, T. C.; Xiong, Q. Room-temperature near-infrared high-Q perovskite whispering-gallery planar nanolasers. *Nano Lett.* **2014**, *14*, 5995−6001.

(10) Deschler, F.; Price, M.; Pathak, S.; Klintberg, L. E.; Jarausch, D.-D.; Higler, R.; Hüttner, S.; Leijtens, T.; Stranks, S. D.; Snaith, H. J.; Atatüre, M.; Phillips, R. T.; Friend, R. H. High photoluminescence efficiency and optically pumped lasing in solution-processed mixed halide perovskite semiconductors. *J. Phys. Chem. Lett.* **2014**, *5*, 1421−1426.

(11) Sambur, J. B.; Novet, T.; Parkinson, B. A. Multiple exciton collection in a sensitized photovoltaic system. *Science* **2010**, *330*, 63−66.

(12) Yang, W. S.; Noh, J. H.; Jeon, N. J.; Kim, Y. C.; Ryu, S.; Seo, J.; Seok, S. I. High-performance photovoltaic perovskite layers fabricated through intramolecular exchange. *Science* **2015**, *348*, 1234−1237.

(13) Ramasamy, P.; Lim, D.-H.; Kim, B.; Lee, S.-H.; Lee, M.-S.; Lee, J.-S. All-inorganic cesium lead halide perovskite nanocrystals for photodetector applications. *Chem. Commun.* **2016**, *52*, 2067−2070.

(14) Xing, J.; Liu, X. F.; Zhang, Q.; Ha, S. T.; Yuan, Y. W.; Shen, C.; Sum, T. C.; Xiong, Q. Vapor phase synthesis of organometal halide perovskite nanowires for tunable room-temperature nanolasers. *Nano Lett.* **2015**, *15*, 4571−4577.

(15) Zhang, J.; Wang, L.; Jiang, C.; Cheng, B.; Chen, T.; Yu, J. $CsPbBr_3$ Nanocrystal Induced Bilateral Interface Modification for Efficient Planar Perovskite Solar Cells. *Adv. Sci.* **2021**, *8*, 2102648.

(16) Villamil Franco, C.; Mahler, B.; Cornaggia, C.; Gustavsson, T.; Cassette, E. Auger Recombination and Multiple Exciton Generation in Colloidal Two-Dimensional Perovskite Nanoplatelets: Implications for Light-Emitting Devices. *ACS Appl. Nano Mater.* **2021**, *4*, 558−567.

(17) Geim, A. K.; Lecture, N. Nobel Lecture: Random walk to graphene. *Rev. Mod. Phys.* **2011**, *83*, 851−862.

(18) Mak, K. F.; Ju, L.; Wang, F.; Heinz, T. F. Optical spectroscopy of graphene: From the far infrared to the ultraviolet. *Solid State Commun.* **2012**, *152*, 1341−1349.

(19) Mak, K. F.; Sfeir, M. Y.; Wu, Y.; Lui, C. H.; Misewich, J. A.; Heinz, T. F. Measurement of the Optical Conductivity of Graphene. *Phys. Rev. Lett.* **2008**, *101*, 196405.

(20) Liu, Y.; Cheng, R.; Liao, L.; Zhou, H.; Bai, J.; Liu, G.; Liu, L.; Huang, Y.; Duan, X. Plasmon resonance enhanced multicolour photodetection by graphene. *Nat. Commun.* **2011**, *2*, 579.

(21) Fei, Z.; Andreev, G. O.; Bao, W.; Zhang, L. M.; McLeod, A. S.; Wang, C.; Stewart, M. K.; Zhao, Z.; Dominguez, G.; Thiemens, M.; Fogler, M. M.; Tauber, M. J.; Castro-Neto, A. H.; Lau, C. N.;

https://doi.org/10.1021/acsomega.2c01310
ACS Omega 2022, 7, 19606−19613

Keilmann, F.; Basov, D. N. Infrared Nanoscopy of Dirac Plasmons at the Graphene−SiO_2 Interface. *Nano Lett.* **2011**, *11*, 4701−4705.
(22) Yan, H.; Li, X.; Chandra, B.; Tulevski, G.; Wu, Y.; Freitag, M.; Zhu, W.; Avouris, P.; Xia, F. Tunable infrared plasmonic devices using graphene/insulator stacks. *Nat. Nanotechnol.* **2012**, *7*, 330−334.
(23) Kloper, V.; Osovsky, R.; Kolny-Olesiak, J.; Sashchiuk, A.; Lifshitz, E. The Growth of Colloidal Cadmium Telluride Nanocrystal Quantum Dots in the Presence of Cd0 Nanoparticles. *J. Phys. Chem. C* **2007**, *111*, 10336−10341.
(24) Smit, M.; van der Tol, J.; Hill, M. Moore's law in photonics. *Laser Photon. Rev.* **2012**, *6*, 1−13.
(25) Blanche, P.-A.; Bablumian, A.; Voorakaranam, R.; Christenson, C.; Lin, W.; Gu, T.; Flores, D.; Wang, P.; Hsieh, W.-Y.; Kathaperumal, M.; Rachwal, B.; Siddiqui, O.; Thomas, J.; Norwood, R. A.; Yamamoto, M.; Peyghambarian, N. Holographic three-dimensional telepresence using large-area photorefractive polymer. *Nature* **2010**, *468*, 80−83.
(26) Johnson, J. C.; Choi, H.-J.; Knutsen, K. P.; Schaller, R. D.; Yang, P.; Saykally, R. J. Single gallium nitride nanowire lasers. *Nat. Mater.* **2002**, *1*, 106−110.
(27) Mondal, N.; De, A.; Samanta, A. All-inorganic perovskite nanocrystal assisted extraction of hot electrons and biexcitons from photoexcited CdTe quantum dots. *Nanoscale* **2018**, *10*, 639−645.
(28) Han, Q.; Wu, W.; Liu, W.; Yang, Y. The peak shift and evolution of upconversion luminescence from $CsPbBr_3$ nanocrystals under femtosecond laser excitation. *RSC Adv.* **2017**, *7*, 35757−35764.
(29) Huang, M. H.; Mao, S.; Feick, H.; Yan, H.; Wu, Y.; Kind, H.; Weber, E.; Russo, R.; Yang, P. Room-temperature ultraviolet nanowire nanolasers. *Science* **2001**, *292*, 1897−1899.
(30) Dohner, E. R.; Jaffe, A.; Bradshaw, L. R.; Karunadasa, H. I. Intrinsic white-light emission from layered hybrid perovskites. *J. Am. Chem. Soc.* **2014**, *136*, 13154−13157.
(31) Kulbak, M.; Cahen, D.; Hodes, G. How Important Is the Organic Part of Lead Halide Perovskite Photovoltaic Cells? Efficient $CsPbBr_3$ Cells. *J. Phys. Chem. Lett.* **2015**, *6*, 2452−2456.
(32) Goldschmidt, V. M. Die gesetze der krystallochemie. *Naturwissenschaften* **1926**, *14*, 477−485.
(33) Li, C.; Lu, X.; Ding, W.; Feng, L.; Gao, Y.; Guo, Z. Formability of ABx_3 (x= F, Cl, Br, I) halide perovskites. *Acta Crystallogr., Sect. B: Struct. Sci.* **2008**, *64*, 702−707.
(34) Green, M. A.; Ho-Baillie, A.; Snaith, H. J. The emergence of perovskite solar cells. *Nat. Photonics* **2014**, *8*, 506−514.
(35) Mitzi, D. B. Templating and structural engineering in organic−inorganic perovskites. *J. Chem. Soc., Dalton Trans.* **2001**, 1−12.

https://doi.org/10.1021/acsomega.2c01310
ACS Omega 2022, 7, 19606−19613